Inorganic Chemistry

Article

pubs.acs.org/IC

# Series of Lanthanide Organometallic Single-Ion Magnets

Shang-Da Jiang, Shan-Shan Liu, Li-Nan Zhou, Bing-Wu Wang,* Zhe-Ming Wang, and Song Gao*

Beijing National Laboratory of Molecular Science, State Key Laboratory of Rare Earth Materials Chemistry and Applications, College of Chemistry and Molecular Engineering, Peking University, Beijing 100871, P. R. China

Supporting Information

**ABSTRACT:** The synthesis, structures, and magnetic properties of a series of lanthanide organometallic mixed sandwich molecules, (Cp*)Ln(COT), are investigated, where Cp* is the pentamethylcyclopentadiene anion and COT is the cyclooctatetraene dianion and Ln represents $Tb^{III}$, $Dy^{III}$, $Ho^{III}$, $Er^{III}$, and $Tm^{III}$. Among the five complexes, Dy and Ho complexes are determined to be single-ion magnets in addition to the previously reported Er complex. Both Dy and Ho complexes show obvious quantum tunneling magnetization relaxation in the absence of a static field. The diluted Ho complex behaves two sets of thermally activated relaxation as we reported previously in Er due to the COT ring static disorder. A stair-shaped hysteresis for the Er compound can be observed at 1.6 K with Hc = 1 kOe at a sweeping rate over 700 Oe/s. The quantum tunneling decoherence relaxation rate increases from Er to Ho to Dy, which may be caused by the relative increase of transverse anisotropy coming from the larger tilting of the two aromatic rings within the molecule. The fine electronic structure is analyzed with ligand-field theory employing the effective Hamiltonian method. The zero-field splitting is determined to be Ising type, and the energy gap between the ground state and the first excited one is consistent with the barrier obtained by Arrhenius analysis.

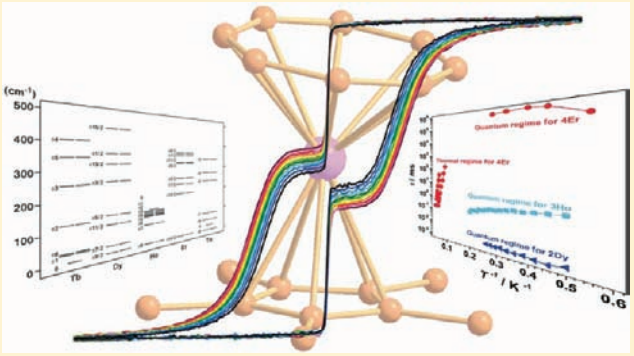

## INTRODUCTION

The crossover of the classical and quantum worlds has been fascinating scientists since the quantum mechanics has been well developed. Molecular nanomagnets provide scientists possible access into the mesoscopic world[1,2] and make it possible to perform a detailed study on the magnetic properties between microscopic and macroscopic materials.[3] The ability of sustaining magnetization like a classical magnet makes molecular nanomagnets act as the target molecule for potential application in high-density information storage.[4] Due to their mesoscopic scale, a molecular nanomagnet is able to have typical magnetization quantum tunneling with a long coherence time,[5−8] which is possible to be applied in quantum computing.[9] To stress the single-molecule feature of a certain sort of molecular nanomagnets, the name single-molecule magnets (SMMs) was suggested and accepted.[10,11]

To improve the blocking temperature of SMMs, as a large amount of investigations have been performed, it is important to increase the relaxation energy barrier which is determined by the uniaxial anisotropy property and ground-state spin multiplicity. It has been reported that some SMMs are discovered with a large ground spin state; nevertheless, the slow relaxation of magnetization does not appear at higher temperature as expected due to the nonobvious uniaxial anisotropy of the whole cluster.[12] The overall uniaxial anisotropy of SMMs, which are normally composed of some paramagnetic centers with uniaxial anisotropy, is often not large and difficult to control for cancellation of the uniaxial anisotropy of individual paramagnetic centers by complex exchange interactions. Besides, the magnetic moments of individual paramagnetic centers of molecules have the tendency to orientate randomly the single-ion anisotropy axes and resulted in a small uniaxial anisotropy. Furthermore, studies on the conditions that determine the anisotropy as well as zero-field splitting properties of a single transition metal or rare earth ions,[13] which is crucial in understanding the nature of the local anisotropy of SMMs, are always confused by the magnetic coupling between spin centers. As a result, it is of great importance to study the SMMs with only one spin carrier, which are also called single-ion magnets (SIMs), to reduce the dimensionality in understanding the electronic structure nature of molecular nanomagnets.

It has been observed that some 3d or 4f isolated metal-ion-containing complexes show a static magnetic field induced thermally activated magnetic relaxation,[14−21] and the absence of slow relaxation without direct current magnetic field is explained by the fast quantum tunneling mechanism.[15,16,20] Due to the prominent spin−orbit coupling effect, several lanthanide-[22−26] and actinide-containing[27] mononuclear molecules were discovered to be SIMs. It was proposed that the high-order single axial ligand field was able to generate the Ising-type degenerated ground state with low-lying excited states in the $10^2$ $cm^{-1}$ energy scale, which can give rise to uniaxial anisotropy and possibly make these molecules behave as high relaxation

**Received:** November 22, 2011
**Published:** February 22, 2012

   dx.doi.org/10.1021/ic202511n | Inorg. Chem. 2012, 51, 3079−3087

Table 1. Crystallographic Data and Structure Refinements for 1Tb, 2Dy, 3Ho, 4Er, 5Tm, and 6Y

| formula | $C_{18}H_{23}Tb$ | $C_{18}H_{23}Dy$ | $C_{18}H_{23}Ho$ | $C_{18}H_{23}Er$ | $C_{18}H_{23}Tm$ | $C_{18}H_{23}Y$ |
|---|---|---|---|---|---|---|
| fw | 398.28 | 401.86 | 404.29 | 406.63 | 408.29 | 328.28 |
| cryst syst | orthorhombic | orthorhombic | orthorhombic | orthorhombic | orthorhombic | orthorhombic |
| space group | *Pnma* | *Pnma* | *Pnma* | *Pnma* | *Pnma* | *Pnma* |
| *a*, Å | 10.3609(2) | 10.3073(2) | 10.2842(2) | 10.2662(8) | 10.2420(3) | 10.2873(3) |
| *b*, Å | 13.2089(3) | 13.2464(3) | 13.2709(3) | 13.3052(13) | 13.3152(4) | 13.2770(3) |
| *c*, Å | 11.9129(3) | 11.8674(2) | 11.8482(3) | 11.8298(11) | 11.8191(3) | 11.8969(4) |
| *V*, Å$^3$ | 1630.35(6) | 1620.31(5) | 1617.05(6) | 1615.9(3) | 1611.82(8) | 1624.93(8) |
| *Z* | 4 | 4 | 4 | 4 | 4 | 4 |
| *T*, K | 293(2) | 293(2) | 293(2) | 293(2) | 293(2) | 293(2) |
| *F*(000) | 784 | 788 | 792 | 796 | 800 | 680 |
| $D_C$, g cm$^{-3}$ | 1.623 | 1.647 | 1.661 | 1.671 | 1.683 | 1.342 |
| $\mu$, mm$^{-1}$ | 4.323 | 4.597 | 4.878 | 5.179 | 5.490 | 3.575 |
| $\lambda$, Å | 0.71073 | 0.71073 | 0.71073 | 0.71073 | 0.71073 | 0.71073 |
| cryst size, mm$^3$ | 0.75 × 0.30 × 0.25 | 0.40 × 0.30 × 0.25 | 0.52 × 0.25 × 0.20 | 0.40 × 0.17 × 0.13 | 0.70 × 0.50 × 0.25 | 0.40 × 0.17 × 0.13 |
| $T_{min}$, $T_{max}$ | 0.231, 0.358 | 0.220, 0.342 | 0.200, 0.411 | 0.231, 0.553 | 0.114, 0.341 | 0.104, 0.320 |
| $\theta_{min}$, $\theta_{max}$, deg | 3.42, 27.49 | 3.43, 27.47 | 3.44, 27.48 | 3.44, 27.46 | 3.45, 27.44 | 3.96, 27.45 |
| R1 [$I \geq 2\sigma(I)$ ] | 0.0242 | 0.0282 | 0.0388 | 0.0321 | 0.0381 | 0.0345 |
| wR2(all data) | 0.0598 | 0.0753 | 0.0823 | 0.0616 | 0.0812 | 0.0823 |
| *S* | 1.022 | 0.880 | 1.060 | 0.863 | 1.295 | 1.028 |
| max and mean $\Delta/\sigma$ | 0.001, 0.000 | 0.001, 0.000 | 0.001, 0.000 | 0.001, 0.000 | 0.001, 0.000 | 0.000, 0.000 |

energy barriers.[22,23] The single-ion feature of these molecular nanomagnets makes them close to the microscopic scale compared with typical cluster-based SMMs, and as a result the quantum aspects seem more prominent in SIMs.[26] Our selection of cyclic polyolefin to construct SIMs is mainly due to the fact that, compared with typical O and N ligands, the coordination of cyclic polyolefin with localized electron pairs to lanthanide may generate higher order uniaxial local symmetry due to the delocalized $\pi$ electrons which can be approximated into a ring of the electron cloud.

Actually, some recent results on lanthanides and actinides confirmed this idea. Significant covalent bonding is reported in a uranium dimer bridged by arene, which is responsible for increasing the blocking temperature.[28] A cyclic polyolefin-sandwiched actinide molecule is determined to have hysteresis as well.[29] We recently reported a single-ion magnet featuring an erbium ion sandwiched by cyclooctatetraene dianion ($C_8H_8^{2-}$, COT) and pentamethylcyclopentadiene anion ($C_5Me_5^-$, Cp*); the relaxation energy barrier was determined to be 323 K, and hysteresis can be observed as high as 5 K.[30] As a continuation of our preliminary study, herein we report detailed studies of this family of single-lanthanide molecules, **1Tb**, **2Dy**, **3Ho**, **4Er**, **5Tm**, and **6Y**, among which **2Dy** and **3Ho** show the SIM behavior in addition to the reported **4Er**. Some new results on the quantum tunneling effect of **4Er** will be presented as well. Ligand-field analysis is performed for all of the studied compounds in detail and provides an explanation for their magnetic behavior from the viewpoint of electronic structure changes.

## RESULTS AND DISCUSSION

**Structure Description.** All crystallographic data and structure refinement results for the complexes are shown in Table 1. Crystal structure analyses show that the six complexes are isomorphous and crystallized in the *Pnma* space group. The crystal cell volumes determined at 293 K for them reduce from 1630 Å$^3$ for **1Tb** to 1612 Å$^3$ for **5Tm** because of the lanthanide contracting effect. The crystal structure for **4Er** is determined at 120, 20, and 10 K, and the cell volume shows a reduction from 1557 Å$^3$ at 120 K to 1535 Å$^3$ at 10 K due to the contraction caused by cooling.

The lanthanide ion is sandwiched by two carbon aromatic rings Cp* and COT (Figure 1a). The COT rings are found to be disordered as they crystallize in two conformations as shown in Figure 1b; the conformer drawn in green is staggered, and the golden one is eclipsed with the ratio refined to be around $W_{staggered}$:$W_{eclipsed}$ = 40:60 throughout the system. The disorder of the COT ring has been observed in the temperature range from 293 to 10 K,[30] indicating its static nature rather than a dynamic origin caused by thermal disturbance.

The nearest neighboring molecules within the *ac* plane are nearly perpendicular to each other with two types of interactions propagating throughout the *ac* plane, edge to face $\pi-\pi$ stacking between COT rings from adjacent molecules,[31] as well as C−H$\cdots\pi$ interaction between the methyl group from Cp* and COT rings[32] as shown in Figure 1c, but no obvious interaction between the *ac* plane can be observed. In both cases of eclipsed COT conformers as either a H-atom donor or an acceptor in the edge to face $\pi-\pi$ stacking the shortest C$\cdots$H distance between the adjacent molecules is favored as shown in Figure S1 and Table S1, Supporting Information, and additionally, more C−H$\cdots\pi$ connections can be found when COT is in the eclipsed conformer (three connections in the eclipsed conformer and two in the staggered one). All of the aforementioned reasons explain that the eclipsed conformer is the major one.

It is interesting that this kind of interaction between adjacent molecules is asymmetric, giving rise to tilting of the mixed sandwich structure as indicated in Figure 1a. The unparallel structure destroys the high uniaxial local symmetry, and the point group of the present tilting mixed sandwich lanthanide molecule is $C_s$. Admitting the existence of an interaction between adjacent molecules, the intermolecular magnetic interaction is negligible due to the long distance between spin carriers in the present system. Taking **5Tm** as an example, whose unit cell is the smallest one among the studied system, the nearest Tm$\cdots$Tm distance is 7.19 Å. The distances of the lanthanides to the aromatic ring and the average metal−carbon bond length are summarized in Table 2. The average bond length of


dx.doi.org/10.1021/ic202511n | Inorg. Chem. 2012, 51, 3079−3087

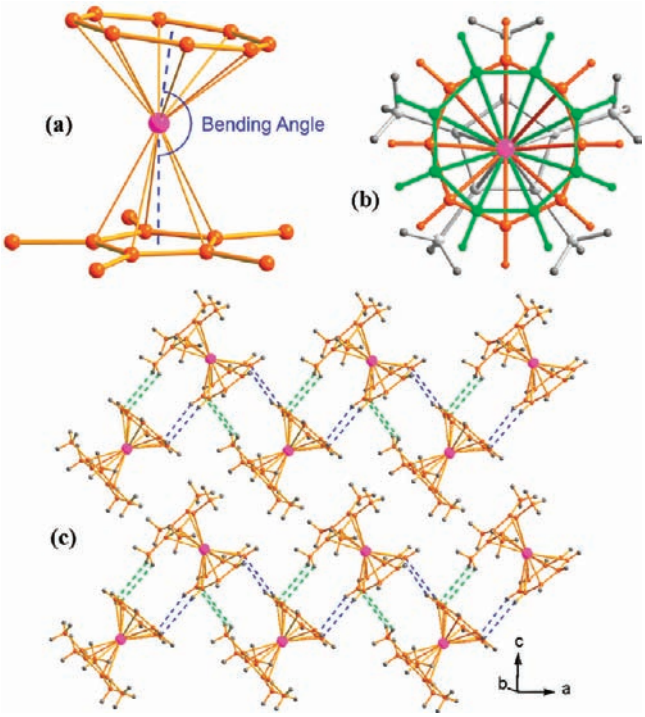


**Figure 1.** (a) Structure of **1Tb**, **2Dy**, **3Ho**, **4Er**, **5Tm**, and **6Y**: pink ball represents lanthanide, and orange balls represent carbon atoms. Hydrogen atoms are omitted for clarity. Blue dashes are the connection between lanthanide and the centroids of the carbon rings. Bending angle is defined as the centroid–lanthanide–centroid angle. (b) Representation of the COT ring disorder: gold ring corresponds to the eclipsed conformer (major), and green ring is the staggered conformer (minor). Bond between Ln (purple) and C from COT is shown in the corresponding color of the conformer. Cp* ring is drawn in gray. (c) Two sorts of stacking interactions propagating throughout the *ac* plane. Edge to face $\pi-\pi$ stacking between COT rings from adjacent molecules is shown with blue dashes, and C–H···$\pi$ between the methyl group from Cp* and the COT rings is indicated with green dashes.

Ln–C(COT) is shorter than that of Ln–C(Cp*) due to the lanthanide sitting closer to the COT plane than to the Cp* plane. This kind of tendency is probably caused by the larger electrostatic attraction from the COT dianion.

**Static Magnetic Properties.** The temperature dependences of the magnetic susceptibilities under static field for **1Tb–5Tm** are collected in the range from 2 to 300 K at 1 kOe. The $\chi_m^{-1}$ vs $T$ plots for all complexes show a linear tendency above 20 K, confirming the paramagnetic single-lanthanide-ion behavior (Figure 2a). The room temperature $\chi_m T$ value is

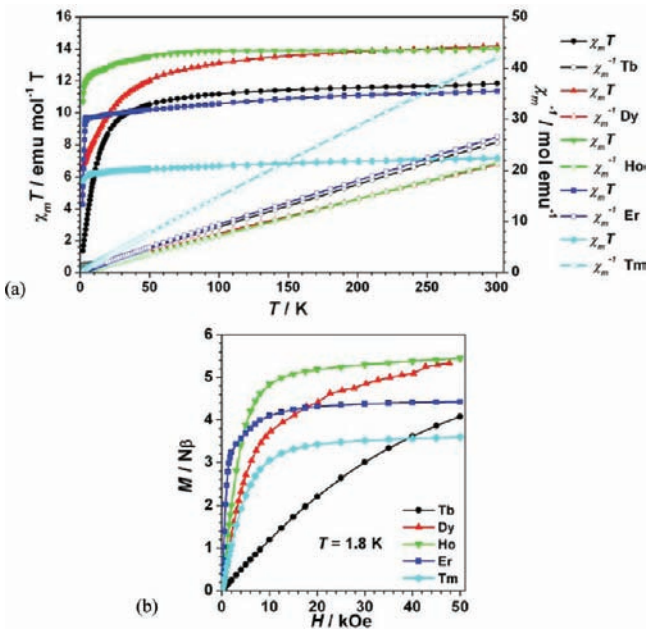


**Figure 2.** Static magnetic properties of the five complexes: (a) plots of $\chi_m T$ and $\chi_m^{-1}$ determined at 1 kOe upon $T$ from 2 to 300 K; (b) plots of magnetization upon magnetic field from 0 to 5 T at 1.8 K.

determined to be 11.83, 14.17, 14.02, 11.47, and 7.15 emu mol$^{-1}$ K for **1Tb**, **2Dy**, **3Ho**, **4Er**, and **5Tm**, respectively, in good agreement with the expected paramagnetic value, 11.82, 14.17, 14.07, 11.48, and 7.15 emu mol$^{-1}$ K for $Tb^{III}$, $Dy^{III}$, $Ho^{III}$, $Er^{III}$, and $Tm^{III}$ (Figure 2a). The downturn of each set of $\chi_m T$ value on cooling can be explained by depopulation of the Stark level split by the ligand field, suggesting the presence of significant magnetic anisotropy. This is confirmed by the magnetization measurement at low temperature. On increasing the static field up to 50 kOe at 1.8 K, the magnetization for **3Ho**, **4Er**, and **5Tm** reaches a value of 5.45, 4.43, and 3.60 N$\beta$, respectively (Figure 2b) and deviates much from theoretical saturation values of 10, 9, and 7 N$\beta$. The magnetization for **1Tb** and **2Dy** keeps increasing at a field of 50 kOe. However, these maximum values are smaller than the expected saturation, which can be attributed to the ligand-field-induced splitting of the Stark level as well as magnetic anisotropy.[34]

**Table 2. Summary of Ionic Radius (picometers), Bond Lengths (Angstroms), Metal to Ring Distances (Angstroms), and Ring–Ring Bending angles (degrees) for 1Tb–5Tm**[a]

| | 1Tb | 2Dy | 3Ho | 4Er | 5Tm | 6Y |
|---|---|---|---|---|---|---|
| ionic radius[b] | 109.5 | 108.3 | 107.2 | 106.2 | 105.2 | 107.5 |
| average Ln–C(Cp*) length | 2.624 | 2.594 | 2.578 | 2.569 | 2.548 | 2.5874 |
| average Ln–C(COT) length | 2.546 | 2.511 | 2.500 | 2.504 | 2.477 | 2.532 |
| Ln to Cp* plane distance | 2.3424(2) | 2.3096(2) | 2.2962(3) | 2.2679(3) | 2.2639(3) | 2.2892(3) |
| Ln to Cp* centroid distance | 2.3326(2) | 2.2995(2) | 2.2815(3) | 2.2676(3) | 2.2438(3) | 2.2896(4) |
| Ln to COT plane distance | 1.8260(2) | 1.7741(2) | 1.7550(3) | 1.7267(3) | 1.7019(3) | 1.7655(4) |
| Ln to COT centroid distance | 1.8250(2) | 1.7728(2) | 1.7529(3) | 1.7265(3) | 1.7017(3) | 1.7653(4) |
| Cp*–COT plane tilting angle | 9.381(113) | 8.324(139) | 7.392(148) | 7.292(190) | 7.169(170) | 7.426(115) |
| centroid–Ln–centroid angle | 170.4 | 171.9 | 173.0 | 174.0 | 173.9 | 173.0 |

[a]Structural data for 1Tb, 2Dy, 3Ho, 5Tm, and 6Y are collected at 293 K. Data for **4Er** is collected at 293 (shown here), 120, 20, and 10 K (available in ref 30). [b]Lanthanide ionic radius are for the nine-coordination situation is from ref 33.


dx.doi.org/10.1021/ic202511n | *Inorg. Chem.* 2012, 51, 3079–3087

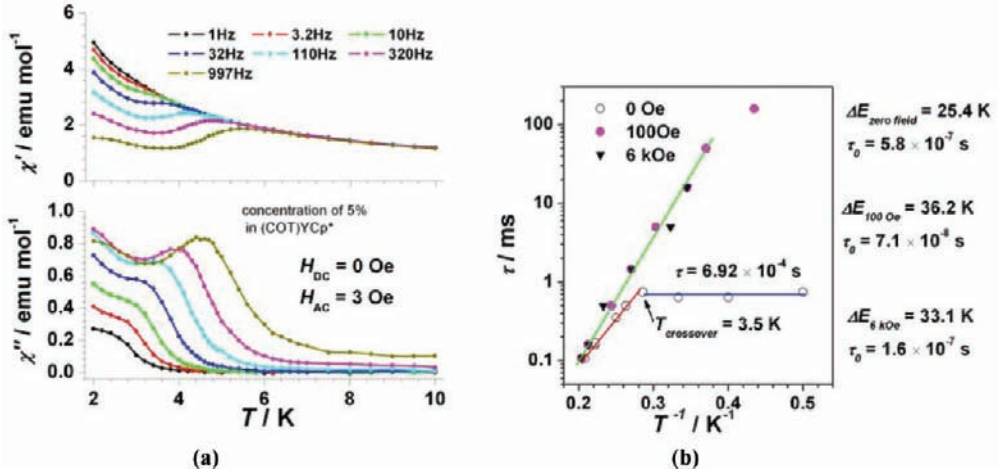


**Figure 3.** Slow relaxation of magnetization for **2Dy** 5% doped in (Cp*)Y(COT): (a) variable-temperature ac susceptibility data at different frequencies in the absence of a static field for diluted **2Dy**; (b) magnetic relaxation time at 0, 100 Oe, and 6 kOe upon temperature and the Arrhenius analyses. Relaxation in the absence of a static field shows a crossover at 3.5 K indicating the coexistence of thermally activated relaxation and quantum tunneling of magnetization relaxation.

**Dynamic Magnetic Properties.** Investigation of the slow magnetization relaxation is carried out via alternative current (ac) susceptibility measurements. Among the series of complexes, **1Tb** and **5Tm** do not show an observable out-of-phase susceptibility signal above 2 K without static field, indicating the absence of slow relaxation of magnetization. However, by applying a static field **5Tm** shows slow relaxation behavior below 5 K while **1Tb** keeps the negligible out-of-phase signal as before (Figure S2, Supporting Information). The fact that these two non-Kramers-ion-containing complexes show different static field-induced dynamic magnetic properties is related to their electronic fine structure as discussed later.

*Dynamic Magnetic Properties of* ***2Dy.*** For the **2Dy** complex, the non-negligible out-of-phase susceptibilities can be recorded and show a frequency dependence in the temperature range from 2 to 10 K (Figure S3, Supporting Information). However, the $\chi''$ signal is as small as no more than 0.1 emu mol$^{-1}$, which is a slight signal compared with the normal reported SIMs. Besides, the $\chi''$ values at all measured frequencies keep increasing on cooling to 2 K without any maximum. By applying a static field of 1 kOe, the $\chi''$ signal is enlarged in a decouple scale, and peaks at a frequency range from 1 to 997 Hz can be observed (Figure S4, Supporting Information). In spite of the former investigation of lanthanide-based SIMs,[26] this phenomenon is proposed to be explained by the suppression of quantum tunneling of magnetization via Zeeman splitting of the degenerate ground Kramers doublets. Due to the limitation of the PPMS instrument, the highest frequency achievable is only 10 000 Hz, which is far lower than the resonant of the quantum tunneling of magnetization; however, by fitting the Argand plots below 4 K in the absence of a static field by the modified Debye model, rough information can be obtained about the quantum tunneling of magnetization relaxation time which is in the $10^{-3}$ ms scale and reamins invariable within the plotting temperature (Figure S5 and Table S2, Supporting Information). For more accurate information, higher frequency or some other experiments are expected.

Considering the isomorphous structure of **6Y** with **4Dy**, the magnetic site dilution experiment was performed to confirm this assumption. The ac susceptibility measurement on the 5% doped sample [(Cp*)$Dy_{0.05}Y_{0.95}$(COT)] without static field shows a clear enlarged out-of-phase signal (Figure 3a). Furthermore, the peak of $\chi''$ signals can even be found at frequencies over 110 Hz. An obvious new increase below the peak temperature can be observed originating from quantum tunneling magnetization as we proposed in our previously studies.[26,30] The Argand plots below 5.5 K without a static field provide us the relaxation times ($\tau$) with corresponding temperatures (Figure S6, Supporting Information). The $\tau$ values show a clear crossover at 3.5 K (Figure 3b). Above the crossing temperature, $\tau$ values obeyed the Arrhenius law with an energy barrier of 25.4 K, indicating the thermally activated mechanism is dominant. However, as the temperature goes below 3.5 K, the $\tau$ value turns to a constant of 0.7 ms, suggesting quantum tunneling of the magnetization process, and the relaxation time can be considered as the quantum decoherence relaxation time corresponding to the change of the magnetic field. Similarly, this quantum tunneling can be suppressed by applying a static field (Figure S7, Supporting Information). The thermally activated relaxation energy barriers are determined to be 36.2 and 33.1 K for 100 Oe and 6 kOe directed field, respectively (Figures 3b and S7, Supporting Information).

*Dynamic Magnetic Properties of* ***3Ho.*** The **3Ho** complex shows a slow relaxation of magnetization in the absence of a static magnetic field. Similar to the **2Dy** case, a frequency dependence of out-of-phase susceptibility can be observed below 20 K; however, the signals at frequencies from 1 to 997 Hz keep increasing on cooling and no peak can be observed (Figure S8, Supporting Information). The Argand plots below 5 K show that the peak frequency of out-of-phase susceptibility has a weak temperature dependence (Figure 4, top). The relaxation time shows a two-regime Arrhenius relationship upon temperature with energy barriers of 7.4 and 3.6 K above and below the temperature of 2.8 K, respectively (Figure S9, Supporting Information). Such small energy barriers and the crossover at 2.8 K indicate the existence of prominent quantum tunneling of magnetization accompanied with thermally activated relaxation. The tunneling decoherence relaxation time is determined to be a little larger than 0.8 ms. By applying a 6 kOe static field, quantum tunneling is suppressed and only thermally activated relaxation can be observed (Figure S10,


dx.doi.org/10.1021/ic202511n | Inorg. Chem. 2012, 51, 3079–3087

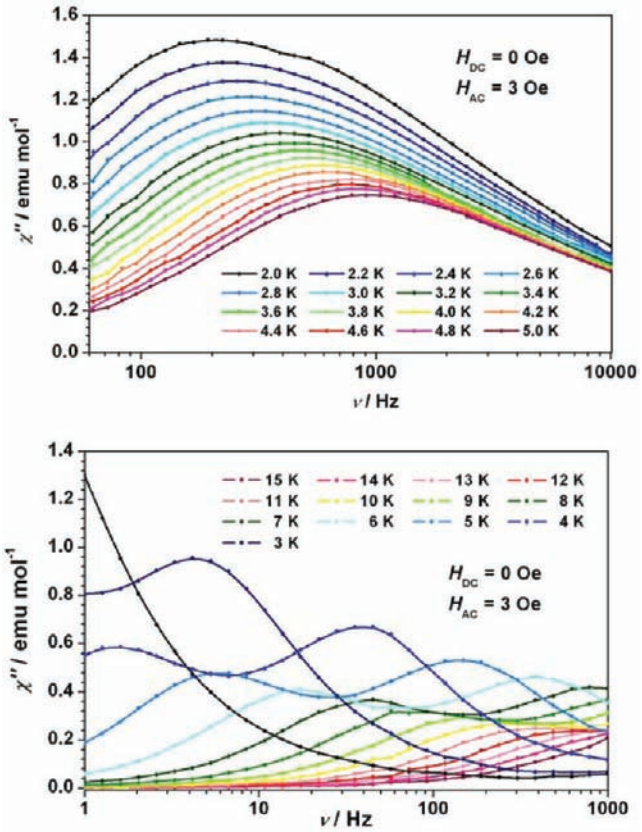


**Figure 4.** Magnetization relaxation at a different temperature range for **3Ho**. (Top) Peaks of the out-of-phase susceptibility versus frequency for **3Ho** show weak temperature dependence below 5 K. (Bottom) Two sets of thermally activated relaxation above 4 K in the absence of a static field for the 5% magnetically diluted **3Ho** sample.

Supporting Information). The magnetic site dilution experiment is able to slow down the tunneling relaxation as well. The ac susceptibility measurement on the 5% doped sample reveals a two-set relaxation process below 20 K (Figures 4, bottom, and S11, Supporting Information). Extracting the relaxation times of both processes, we are able to perform an Arrhenius analysis and two thermally activated relaxation processes with energy barriers of 33.8 and 24.4 K can be concluded (Figure S12, Supporting Information). This kind of two-set thermally activated relaxation behavior is quiet similar with the prior one reported for **4Er** complexes.[30] As discussed in previous work, two-set relaxation process can be described by a linear combination of two modified Debye models given by eq 1.[35]

$$\chi_{total}(\omega) = \chi_S + (\chi_T - \chi_S)\left[\frac{\beta}{1 + (i\omega\tau_1)^{1-\alpha_1}} + \frac{1-\beta}{1 + (i\omega\tau_2)^{1-\alpha_2}}\right] \quad (1)$$

In the equation, $\chi_S = \chi_{\omega\to\infty}$ is the adiabatic susceptibility, $\chi_T = \chi_{\omega\to 0}$ is the isothermal susceptibility, $\omega = 2\pi f$ is the angular frequency, $\tau_1$ and $\tau_2$ are the magnetization of the two parts, $\alpha_1$ and $\alpha_2$ describe the distribution of relaxation corresponding to the two parts, respectively, and $\beta$ is the weight of the first relaxation process; thus, $(1 - \beta)$ corresponds to the second one. Separating the real and imaginary parts, one obtains $\chi'$ and $\chi''$ as eqs 2 and 3.

$$\chi' = \chi_S + (\chi_T - \chi_S) \times \left\{\frac{\beta\left[1 + (\omega\tau_1)^{1-\alpha_1}\sin\left(\frac{1}{2}\alpha_1\pi\right)\right]}{1 + 2(\omega\tau_1)^{1-\alpha_1}\sin\left(\frac{1}{2}\alpha_1\pi\right) + (\omega\tau_1)^{2(1-\alpha_1)}} + \frac{(1-\beta)\left[1 + (\omega\tau_2)^{1-\alpha_2}\sin\left(\frac{1}{2}\alpha_2\pi\right)\right]}{1 + 2(\omega\tau_2)^{1-\alpha_2}\sin\left(\frac{1}{2}\alpha_2\pi\right) + (\omega\tau_2)^{2(1-\alpha_2)}}\right\} \quad (2)$$

$$\chi'' = (\chi_T - \chi_S) \times \left\{\frac{\beta(\omega\tau_1)^{1-\alpha_1}\cos\left(\frac{1}{2}\alpha_1\pi\right)}{1 + 2(\omega\tau_1)^{1-\alpha_1}\sin\left(\frac{1}{2}\alpha_1\pi\right) + (\omega\tau_1)^{2(1-\alpha_1)}} + \frac{(1-\beta)(\omega\tau_2)^{1-\alpha_2}\cos\left(\frac{1}{2}\alpha_2\pi\right)}{1 + 2(\omega\tau_2)^{1-\alpha_2}\sin\left(\frac{1}{2}\alpha_2\pi\right) + (\omega\tau_2)^{2(1-\alpha_2)}}\right\} \quad (3)$$

Fitting the Cole−Cole plots between 4 and 8 K in the absence of a static field with eqs 2 and 3 the relaxation weight ratio $\beta/(1 - \beta)$ can be obtained (Figure S13, Supporting Information). The results reveal that in the temperature range from 4 to 8 K the ratio reamins unaltered as 0.4(1)/0.6(1), which is consistent with the ratio of the two conformers (0.32/0.68) that gives rise to static disorder (Table S3, Supporting Information). It is indicated that the static disorder is responsible for the two thermally activated relaxation processes just as in the **4Er** case.[30]

*Dynamic Magnetic Properties of 4Er.* The dynamic susceptibility of **4Er** has been described in detail in a previous communication.[30] The complex has double thermally activated relaxation processes in the temperature range from 10 to 30 K with energy barriers of 323 and 197 K, which are among the highest ones with regard to the SIMs based on lanthanide. Furthermore, there is a slow quantum tunneling of magnetization below 10 K with a quantum decoherence relaxation time on the $10^2$ s scale. Such a long magnetization tunneling relaxation time, as well as the large energy barriers corresponding to the thermally activated relaxation, gives rise to the evident hysteresis loop recorded at a persistent mode at 1.8 K or even up to 5 K. However, the hysteresis has a butterfly shape without any non-neglected coercive field or remanence, and this was attributed to the magnetization tunneling effect at zero static field.

To confirm this assumption, we recorded the hysteresis loops of powder samples at 1.6 K in a continuously-field-sweeping mode on the SQUID-VSM produced by Quantum Design. The direct field was generated via a superconducting magnet up to 70 kOe with a sweeping rate as high as 700 Oe/s. According to the theory of nonadiabatic transition between two states developed by Landau,[36] Zener,[37] and Stückelberg,[38] the tunneling probability can be diminished via increasing the field sweeping rate.[39] Experimentally, the various coercive fields are indeed observed


dx.doi.org/10.1021/ic202511n | Inorg. Chem. 2012, 51, 3079−3087

with sweeping rates over 100 Oe/s, and the larger coercive field is favored by the higher sweeping rate (Figure 5, top). This

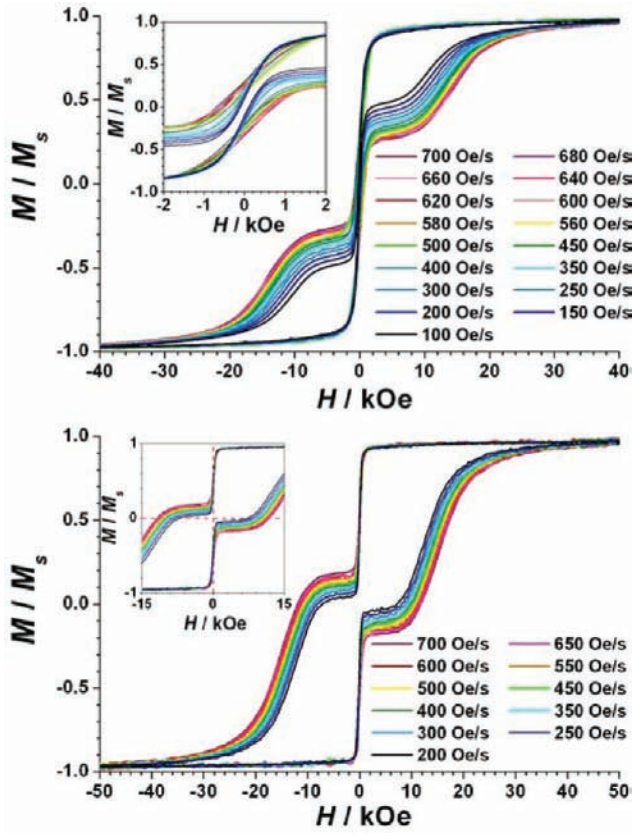


**Figure 5.** Hysteresis loops at 1.6 K at various static field sweeping rates measured on the powder sample of **4Er** (top) and its 5% diluted sample (bottom).

behavior demonstrates that the quantum tunneling of magnetization mechanism is responsible for the absence of a coercive field in persistent mode. Murugesu and co-workers recently presented research demonstrating that the magnetic site doping is able to suppress the tunneling of magnetization,[40] and we concluded similar accounts.[26] Herein the hysteresis in sweeping mode is performed on a 5% doped **4Er** sample as well, and a coercive field as large as 13 kOe at a sweeping rate of 700 Oe/s can be recorded (Figure 5, bottom).

**Quantum Tunneling of Magnetization.** Figure 6 summarizes the quantum tunneling decoherence relaxation time for **2Dy** ($10^{-3}$ ms), **3Ho** ($10^{-1}$ ms), and **4Er** ($10^{6}$ ms), respectively. It is easy to find that this happens to be the sequence of ionic radius with respect to the lanthanide contraction effect. In order to explore the effects that determine the above sequence, the structural differences between the series of isomorphous crystals are studied in detail.

As described previously due to the asymmetrical packing in the crystal, the two aromatic rings within one molecule are not perfectly parallel to each other. It is convenient to describe the bending of the axis through the lanthanide by calculating the centroid(Cp*)−Ln−centroid(COT) angle as listed in Table 2. It has already been concluded that for the structure of $Cp^*_2M$, where M represents an alkaline earth metal ion as well as a divalent lanthanide, the bending of the axis increases with the increment of ionic radius of M.[41] This is similar in the alkaline earth dihalide structures.[42−44] Evans summarized that the

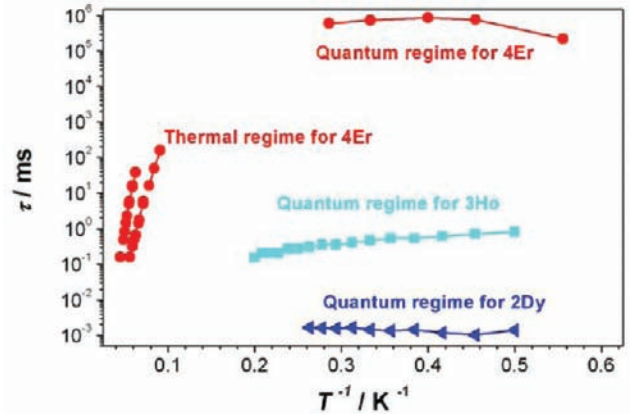


**Figure 6.** Relaxation rate of magnetization for **2Dy**, **3Ho**, and **4Er** at various temperatures. Relaxation time in quantum regime varies in large scale from **2Dy** to **4Er**.

bending of the mixed sandwich structure, (Cp*)Ln(COT), is favored by larger metals.[45] In addition to his results, we plot the bending angle versus ionic radius in Figure 7 and a nearly linear

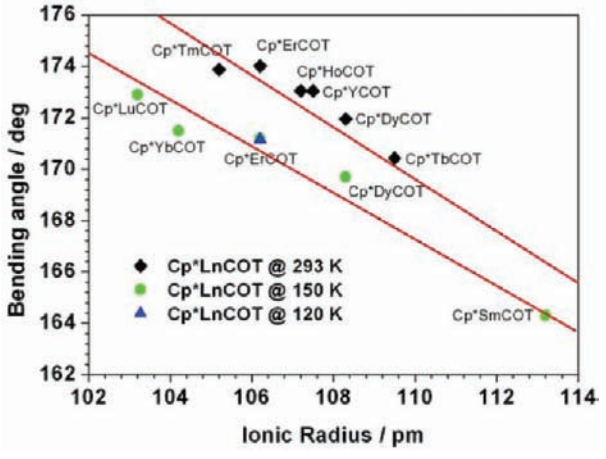


**Figure 7.** Plots of bending angles of (Cp*)Ln(COT) upon ionic radius; lanthanide ionic radius for the nine-coordination situation are from ref 33. Black plots are calculated from structures determined at 293 K in this work. Green plots are from structures determined at 150 K by Evans and co-workers in previous work.[45] Blue plots are from our previous communication.[30]

relationship can be obtained. The bending angles were determined at 150 K in Evans' work, and a slight difference of no more than 2° can be discovered when the temperature increases to 293 K in the present situation. A nearly linear relationship between the bending angle and the lanthanide ionic radius can be observed at both temperatures, and it is clear that the bending angle increases with the increment of ionic radius. The bending of the two aromatic rings destroys the high local symmetry of the lanthanide and introduces transverse anisotropy with respect to the bending angle into the system.

The ligand field of uniaxial symmetry is probably able to split the microstates into Ising type, giving rise to the bistable states as well as the slow relaxation of magnetization. For a strict Ising-type zero-field splitting without any perturbation Hamiltonian such as transverse anisotropy, hyperfine interaction, or dipole−dipole interaction, etc., the split states are orthogonal to each other and no tunneling of magnetization


dx.doi.org/10.1021/ic202511n | Inorg. Chem. 2012, 51, 3079−3087

can be observed.[5] In other words, the wave function of the system is localized in one of the ground states with respect to the time-dependent Schrödinger equation. However, once the unavoidable perturbation Hamiltonian that does not commute with $\hat{S}_z$ or $\hat{J}_z$, e.g., transverse anisotropy, is introduced, the states are not orthogonal any more and mixed by the perturbation. Alternately, we can say the wave function is delocalized between the two ground states as described in eq 4, where $\delta E$ refers to the tunneling splitting determined by the perturbation.

$$|\Psi(t)\rangle = e^{iEt/\hbar}\left[\cos\left(\frac{t\delta E}{\hbar}\right)|+J\rangle - i\sin\left(\frac{t\delta E}{\hbar}\right)|-J\rangle\right] \quad (4)$$

It can be concluded from eq 4 that the larger the perturbation is, the easier tunneling of magnetization is able to happen and the faster the quantum decoherence relaxation is. The aforementioned structural analyses reveal that the bending of the axis through the lanthanide, which is one of the major sources introducing transverse anisotropy, is favored by a larger metal ion radius. According to the discussion above, it is reasonable to conclude that the larger lanthanide ion radius is probably the cause of faster quantum tunneling of magnetization between ground states. It is indeed the case in this series of complexes. Nevertheless, it should be mentioned that transverse anisotropy is only one of the perturbation sources, and there are probably some other reasons responsible for the present tunneling relaxation sequence due to the different electronic structures between lanthanide ions; what we discussed here is just a steric structure effect accounting for the present observations.

The existence of the bending angle can probably explain the two thermally activated energy barriers of the eclipsed and staggered conformers. As can be seen in Table S1, Supporting Information, the bending angles for the two conformers show a slight difference, which may cause a divergence for the tunneling rate, and consequently, changes in the Arrhenius determined energy barriers for the thermally activated energy level can always be reduced via quantum tunneling of magnetization.[5]

**Electronic Fine Structure Determination.** It is beyond doubt of crucial importance to obtain the electronic fine structure information for understanding the magnetic properties of the lanthanide-containing system. However, determining the splitting of the sublevel is a difficult task for both experimental and theoretical experts.[46] Different from the 3d ions' case, the orbit contribution is always obviously affecting the magnetic properties of the lanthanide except for the spin-only $f^7$ configuration. The strong spin−orbit coupling of the lanthanide makes the total angular momentum $J$ rather than $S$ a well-defined quantum number. Then the electronic states are split further into Stark sublevels by the ligand field. Because of the 4f orbital shielded by 5d, 6s orbitals, the ligand-field splitting is only on the scale of several hundred wave numbers, which is comparable to thermal fluctuation. The temperature dependence of the magnetic susceptibility reflects the thermal population of the split ground multiplets and offers a way to approach the electronic fine structure of the lanthanide.

Ishikawa developed a method based on this idea to determine the electronic fine structure of a series of isostructural lanthanide complexes,[47] and this method is proven to be effective in explaining the magnetic properties of SIMs[23,25,48] as well as the static magnetic field-induced slow relaxation phenomenon.[20] Lueken and co-workers introduced the spin−orbit coupling, ligand-field, as well as Zeeman term into the fitting Hamiltonian in addition to interelectronic repulsion and developed the program code CONDON,[49] which offers us the possibility to obtain the electronic structures of a few d and f systems including the mononuclear lanthanide with high local symmetry. In addition to the most commonly used Stevens notation[50] with an equivalent operator method, the ligand-field term in CONDON can be described by Wybourne notation[51] as well. The Wybourne notation of the ligand field enables us to employ the full basis of microstates, which can be more accurate and effective in describing the electronic fine structures, instead of the Russell−Saunders coupled basis to take into iteration. The model Hamiltonian for a single lanthanide ion complex can be expressed as in eq 5.

$$\hat{H} = \hat{H}_0 + \hat{H}_{ee} + \hat{H}_{SO} + \hat{H}_{LF} + \hat{H}_{mag} \quad (5)$$

By approximating the bending angle described in Figure 1a into 180° and considering the delocalized $\pi$-type electron cloud on both ligands, the local symmetry of the central lanthanide can be regarded as $C_{\infty v}$. Fitting the static magnetic susceptibility of **1Tb**, **2Dy**, **3Ho**, **4Er**, and **5Tm** from 20 to 300 K measured at 1 kOe into eq 5 of $C_{\infty v}$ ligand-field symmetry, one is able to obtain the Stark levels of each complex (Figure S14, Supporting Information). The fine electronic spectra are given in Figure 8,

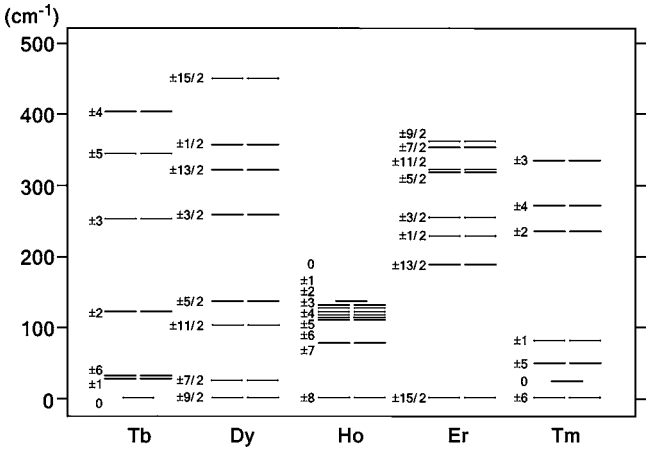


**Figure 8.** Fine electronic spectra of **1Tb**, **2Dy**, **3Ho**, and **5Tm** simulated from the CONDON program. Spectrum of **4Er** is reproduced corresponding to the one reported previously. Only the low-lying levels split from the ground $^{2S+1}L_J$ are listed. $M_J$ values for the corresponding states are shown on the left side of each level.

and only the low-lying levels split from the ground $^{2S+1}L_J$ are listed.

As can be seen from the energy spectra, only **2Dy**, **3Ho**, and **4Er** behave with typical Ising ground states with an allowed transition which give rise to their SIM behavior. The ground state of **5Tm** is the largest projection of angular momentum with $M_J = \pm 6$; nevertheless, the first excited state is the singlet one with $M_J = 0$ and the transition of the lowest two states is forbidden; as a result no slow relaxation in the absence of a static field can be observed. The energy gaps between the ground states and the first excited states of the three SIMs are determined to be 24.3 (34.9 K), 80.6 (115.9 K), and 189.4 $cm^{-1}$(272.4 K) for **2Dy**, **3Ho**, and **4Er**, respectively, which are closed to the energy barriers from Arrhenius analyses. This accordance indicates that the relaxation processes of the three SIMs are probably via the Orbach process between the two lowest lying states.


dx.doi.org/10.1021/ic202511n | Inorg. Chem. 2012, 51, 3079−3087

Furthermore, as described, the two non-Kramers ion-containing complexes **1Tb** and **5Tm** show different relaxation behavior with the existence of a static field. **5Tm** is able to behave in the static field, inducing slow relaxation of magnetization, while **1Tb** cannot. It can be ascribed to the different degeneracy of ground states of these two compounds, which is determined to be singlet for **1Tb** while the one of **5Tm** is doublet. This is quite similar with the case of $[Ln(dipic)_3]^{3-}$ (dipic = pydine-2,6,-dicarboxylate) reported by Ishikawa and co-workers.[20] The field-induced slow relaxation can be probably explained by the field, eliminating fast tunneling between degenerate doublets in **5Tm**, which is not effective for the singlet ground state in **1Tb**.

## CONCLUSION

We studied the crystal structures and magnetic properties of a series of lanthanide organometallic mixed sandwich molecules. These complexes have been characterized by X-ray crystallography and static and dynamic susceptibility measurements. Among the six complexes **2Dy**, **3Ho**, and **4Er** are determined to be single-ion magnets. The **2Dy** and **3Ho** complexes mainly show quantum tunneling relaxation in the absence of a static field. The magnetic site diluted **2Dy** complex shows a crossover at a temperature of 3.5 K from thermally activated relaxation to quantum tunneling relaxation on cooling, and the diluted **3Ho** sample has two sets of thermally activated relaxation as we reported previously in the **4Er** case. By changing the field-sweeping rate the hysteresis measurement performed on **4Er**, and its diluted sample showed stair-like loops at a temperature of 1.6 K. The quantum tunneling decoherence relaxation rates increases from **4Er** to **3Ho** to to **2Dy**, which may be caused by the more evident transverse anisotropy origin from the tilting of the two aromatic rings within one molecule. Ligand-field analyses reveal that the Ising-type ground state of **2Dy**, **3Ho**, and **4Er** can give rise to the single-ion magnet behavior. Taken together, these studies establish a class of typical single-ion magnets based on lanthanide, and the collective structure as well as the magnetic properties provide a starting point for further studies on this sort of sandwiched mononuclear magnets, such as their single-molecule and monolayer behaviors on the surface.

## EXPERIMENTAL SECTION

**Synthesis.** *(COT)LnCl(thf)$_x$.* This was prepared according to the literature procedure[52] with slight modifications and the syntheses were taken in a nitrogen-filled glovebox or by traditional Schlenk techniques, the tetrahydrofurane (THF) and toluene were dried in solvent purification system. Cyclooctatetraene (COT) was bought from Alfa Aesar and degassed after dried over activated 4 Å molecular sieves overnight. $LnCl_3$ was bought from Strem without further purification. The complex was synthesized by using the method of Wayda with slight alternations.[52] Adding the cyclooctatetraene (10 mmol in 20 mL THF) to a stirred suspension of freshly cut potassium (20 mmol) in 10 mL THF generates a dark brown solution, which is filtered after all the potassium is solved. Slow addition of the filtrate to a violently stirred suspension of solvated anhydrous $LnCl_3$ (10 mmol) in 20 mL THF in an hour produces an orange color slurry which is stirred for 24 h to complete the reaction. After removal of the solvent, the crude product is purified by extraction with 100 mL THF by a Soxhlet extraction apparatus on Schlenk line in nitrogen over a 12-h period. During the extraction, the slightly soluble product solid is collected in the Soxhlet receiver flask, which is isolated in the glovebox.

*(Cp*)Ln(COT).* The complex was synthesized by the method of Schumann[53] with slight modification. A 0.82 mmol amount of NaCp* solvated in 5 mL of THF was added dropwise into a suspension of 0.67 mmol of $(COT)LnCl(thf)_x$ in 15 mL of THF. Solvent was removed after 24 h of stirring, and the residue was extracted with 10 mL of toluene and filtered. The solution was concentrated to 3 mL and refiltered. The filtrate was cooled to −30 °C overnight, and crystals were collected. The magnetic site 20-time dilution complex is synthesized by adding a mole ratio 19: 1 of $(COT)YCl(thf)_x$ and $(COT)LnCl(thf)_x$ together, reacting with a corresponding amount of NaCp*. **1Tb**: yield 56.0%. Anal. Calcd for $C_{18}H_{23}Tb$: C, 54.27; H, 5.82. Found: C, 54.20; H, 5.84. **2Dy**: yield 54.7%. Anal. Calcd for $C_{18}H_{23}Dy$: C, 53.80; H, 5.77. Found: C, 53.72; H, 5.77. **3Ho**: yield 51.2%. Anal. Calcd for $C_{18}H_{23}Ho$: C, 53.47; H, 5.73. Found: C, 53.44; H, 5.77. **5Tm**: yield 54.7%. Anal. Calcd for $C_{18}H_{23}Tm$: C, 52.95; H, 5.68. Found: C, 52.42; H, 5.67.

**Crystal Structure Determination.** Data were collected on a Nonius KappaCCD diffractometer with Mo K$\alpha$ radiation ($\lambda$ = 0.71073 Å). Empirical absorption corrections were applied using the Sortav program. All structures were solved by direct methods and refined by full-matrix least-squares on $F^2$ using the SHELX program. H atoms can be located from the difference Fourier synthesis but added according to the ideal geometry and not refined for good refinement convergence. Crystallographic data and structure refinement results are listed in Table 1.

**Magnetic Properties Measurement.** Samples were fixed by eicosane to avoid moving during measurement and sealed in an NMR tube to avoid reaction with moisture and oxygen in the air. Direct current susceptibility and alternative current susceptibility with frequencies in the range from 1 to 997 Hz were performed on a Quantum Design MPMS XL-5 SQUID magnetometer on polycrystalline samples. Alternative current susceptibility with frequencies in the range from 10 to 10000 Hz was performed on a Quantum Design PPMS magnetometer on polycrystalline samples. The hysteresis loops at 1.6 K with a sweeping rate in the range from 100 to 700 Oe/s are collected on a Quantum Design SQUID-VSM magnetometer on polycrystalline samples. Data were corrected for the diamagnetism of the samples using Pascal constants and the sample holder by measurement.

## ASSOCIATED CONTENT

### Supporting Information

Additional ac susceptibility data for **1Tb**, **2Dy**, **3Ho**, and **5Tm** and their dilution sample, Argand plots fitting to a two-set linear combination of a modified Debye model, CONDON program fitting of the static susceptibility data for **1Tb**, **2Dy**, **3Ho**, **4Er**, and **5Tm**, CIF files for **1Tb**, **2Dy**, **3Ho**, **4Er**, **5Tm**, and **6Y** determined at 293 K. This material is available free of charge via the Internet at http://pubs.acs.org.

## AUTHOR INFORMATION

### Corresponding Author

*E-mail: bwwang@pku.edu.cn (B.-W.W.); gaosong@pku.edu.cn (S.G.).

### Notes

The authors declare no competing financial interest.

## ACKNOWLEDGMENTS

We thank the National Science Foundation of China (20821091, 90922033, and 21071008) and the National Basic Research Program of China (2009CB929403, 2010CB934601) for support. We also thank Mr. Yan Zhang in the College of Physics, Peking University, and Mr. Dong-Wei Wang in the National Center for Nanoscience and Technology (NCNST) of China for the Physical Properties Measurement System operation. We appreciate the help from Mr. Shao-Kui Su from the Institute of Physics CAS for SQUID-VSM measurement.

## REFERENCES


(1) Sessoli, R.; Tsai, H. L.; Schake, A. R.; Wang, S. Y.; Vincent, J. B.; Folting, K.; Gatteschi, D.; Christou, G.; Hendrickson, D. N. *J. Am. Chem. Soc.* **1993**, *115*, 1804.

(2) Gatteschi, D.; Sessoli, R.; Villain, J. *Molecular Nanomagnets*; Oxford University Press: New York, 2006.

(3) Barbara, B.; Thomas, L.; Lionti, F.; Chiorescu, I.; Sulpice, A. *J. Magn. Magn. Mater* **1999**, *200*, 167.

(4) Sessoli, R.; Gatteschi, D.; Caneschi, A.; Novak, M. A. *Nature* **1993**, *365*, 141.

(5) Gatteschi, D.; Sessoli, R. *Angew. Chem., Int. Ed.* **2003**, *42*, 268.

(6) Friedman, J. R.; Sarachik, M. P.; Tejada, J.; Ziolo, R. *Phys. Rev. Lett.* **1996**, *76*, 3830.

(7) Thomas, L.; Lionti, F.; Ballou, R.; Gatteschi, D.; Sessoli, R.; Barbara, B. *Nature* **1996**, *383*, 145.

(8) Wernsdorfer, W.; Sessoli, R. *Science* **1999**, *284*, 133.

(9) Jones, J. A. *Science* **1998**, *280*, 229.

(10) Eppley, H. J.; Aubin, S. M. J.; Wemple, M. W.; Adams, D. M.; Tsai, H. L.; Grillo, V. A.; Castro, S. L.; Sun, Z. M.; Folting, K.; Huffman, J. C.; Hendrickson, D. N.; Christou, G. *Mol. Cryst. Liq. Cryst. A* **1997**, *305*, 167.

(11) Aubin, S. M. J.; Spagna, S.; Eppley, H. J.; Sager, R. E.; Folting, K.; Christou, G.; Hendrickson, D. N. *Mol. Cryst. Liq. Cryst. A* **1997**, *305*, 181.

(12) Ako, A. M.; Hewitt, I. J.; Mereacre, V.; Clerac, R.; Wernsdorfer, W.; Anson, C. E.; Powell, A. K. *Angew. Chem., Int. Ed.* **2006**, *45*, 4926.

(13) Gatteschi, D.; Sorace, L. *J. Solid State Chem.* **2001**, *159*, 253.

(14) Liu, Q.-D.; Li, J. R.; Gao, S.; Ma, B.-Q.; Zhou, Q.-Z.; Yu, K.-B.; Liu, H. *Chem. Commun.* **2000**, 1685.

(15) Freedman, D. E.; Harman, W. H.; Harris, T. D.; Long, G. J.; Chang, C. J.; Long, J. R. *J. Am. Chem. Soc.* **2010**, *132*, 1224.

(16) Harman, W. H.; Harris, T. D.; Freedman, D. E.; Fong, H.; Chang, A.; Rinehart, J. D.; Ozarowski, A.; Sougrati, M. T.; Grandjean, F.; Long, G. J.; Long, J. R.; Chang, C. J. *J. Am. Chem. Soc.* **2010**, *132*, 18115.

(17) Yi, T.; Gao, S.; Li, B.-G. *Polyhedron* **1998**, *17*, 2243.

(18) Ma, B.-Q.; Gao, S.; Su, G.; Xu, G.-X. *Angew. Chem., Int. Ed.* **2001**, *40*, 434.

(19) Gao, S.; Su, G.; Yi, T.; Ma, B.-Q. *Phys. Rev. B* **2001**, *63*, 054431.

(20) Sugita, M.; Ishikawa, N.; Ishikawa, T.; Koshihara, S.; Kaizu, Y. *Inorg. Chem.* **2006**, *45*, 1299.

(21) Zhang, Y.-Z.; Duan, G.-P.; Sato, O.; Gao, S. *J. Mater. Chem.* **2006**, *16*, 2625.

(22) Ishikawa, N.; Sugita, M.; Ishikawa, T.; Koshihara, S.; Kaizu, Y. *J. Am. Chem. Soc.* **2003**, *125*, 8694.

(23) Ishikawa, N.; Sugita, M.; Ishikawa, T.; Koshihara, S.; Kaizu, Y. *J. Phys. Chem. B* **2004**, *108*, 11265.

(24) AlDamen, M. A.; Clemente-Juan, J. M.; Coronado, E.; Marti-Gastaldo, C.; Gaita-Arino, A. *J. Am. Chem. Soc.* **2008**, *130*, 8874.

(25) AlDamen, M. A.; Cardona-Serra, S.; Clemente-Juan, J. M.; Coronado, E.; Gaita-Arino, A.; Marti-Gastaldo, C.; Luis, F.; Montero, O. *Inorg. Chem.* **2009**, *48*, 3467.

(26) Jiang, S.-D.; Wang, B.-W.; Su, G.; Wang, Z.-M.; Gao, S. *Angew. Chem., Int. Ed.* **2010**, *49*, 7448.

(27) Rinehart, J. D.; Long, J. R. *J. Am. Chem. Soc.* **2009**, *131*, 12558.

(28) Mills, D. P.; Moro, F.; McMaster, J.; van Slageren, J.; Lewis, W.; Blake, A. J.; Liddle, S. T. *Nat. Chem.* **2011**, *3*, 454.

(29) Magnani, N.; Apostolidis, C.; Morgenstern, A.; Colineau, E.; Griveau, J.-C.; Bolvin, H.; Walter, O.; Caciuffo, R. *Angew. Chem., Int. Ed.* **2011**, *50*, 1696.

(30) Jiang, S.-D.; Wang, B.-W.; Sun, H.-L.; Wang, Z.-M.; Gao, S. *J. Am. Chem. Soc.* **2011**, *133*, 4730.

(31) Hunter, C. A.; Sanders, J. K. M. *J. Am. Chem. Soc.* **1990**, *112*, 5525.

(32) Desiraju, G. R.; Steiner, T. *The Weak Hydrogen Bond in Structural Chemistry and Biology*; Oxford University Press: New York, 1999.

(33) Evans, W. J. *Inorg. Chem.* **2007**, *46*, 3435.

(34) Tang, J. K.; Hewitt, I.; Madhu, N. T.; Chastanet, G.; Wernsdorfer, W.; Anson, C. E.; Benelli, C.; Sessoli, R.; Powell, A. K. *Angew. Chem., Int. Ed.* **2006**, *45*, 1729.

(35) Domingo, N.; Luis, F.; Nakano, M.; Munto, M.; Gomez, J.; Chaboy, J.; Ventosa, N.; Campo, J.; Veciana, J.; Ruiz-Molina, D. *Phys. Rev. B* **2009**, *79*, 214404.

(36) Landau, L. *Phys. Z.* **1932**, *2*, 46.

(37) Zener, C. *Proc. R. Soc. London, Ser. A* **1932**, *137*, 696.

(38) Stückelberg, E. C. G. *Helv. Phys. Acta* **1932**, *5*, 369.

(39) Wernsdorfer, W. *C. R. Chim.* **2008**, *11*, 1086.

(40) Habib, F.; Lin, P.-H.; Long, J. r. m.; Korobkov, I.; Wernsdorfer, W.; Murugesu, M. *J. Am. Chem. Soc.* **2011**, *133*, 8830.

(41) Burkey, D. J.; Hanusa, T. P. *Comments Inorg. Chem.* **1995**, *17*, 41.

(42) Buchler, A.; Stauffer, J. L.; Klemperer, W. *J. Am. Chem. Soc.* **1964**, *86*, 4544.

(43) Balducci, G.; Gigli, G.; Guido, M. *J. Chem. Phys.* **1979**, *70*, 3146.

(44) Kaupp, M.; Schleyer, P. V.; Dolg, M.; Stoll, H. *J. Am. Chem. Soc.* **1992**, *114*, 8202.

(45) Evans, W. J.; Johnston, M. A.; Clark, R. D.; Ziller, J. W. *J. Chem. Soc., Dalton Trans.* **2000**, *10*, 1609.

(46) Sorace, L.; Benelli, C.; Gatteschi, D. *Chem. Soc. Rev.* **2011**, *40*, 3092.

(47) Ishikawa, N.; Iino, T.; Kaizu, Y. *J. Phys. Chem. A* **2002**, *106*, 9543.

(48) Ishikawa, N.; Sugita, M.; Okubo, T.; Tanaka, N.; Lino, T.; Kaizu, Y. *Inorg. Chem.* **2003**, *42*, 2440.

(49) Schilder, H.; Lueken, H. *J. Magn. Magn. Mater* **2004**, *281*, 17.

(50) Stevens, K. W. H. *Proc. R. Soc. London, Ser. A* **1952**, *65*, 209.

(51) Wybourne, B. G. *Spectroscopic Properties of Rare Earths*; Wiley: New York, 1965.

(52) Wayda, A. L. *Organometallics* **1983**, *2*, 565.

(53) Schumann, H.; Kohn, R. D.; Reier, F. W.; Dietrich, A.; Pickardt, J. *Organometallics* **1989**, *8*, 1388.